Perceptual consequences of retinal stabilization with high-frequency non-stroboscopic displays

Y. Howard Li
Department of Brain and Cognitive Sciences, University of Rochester, NY, USA
Center for Visual Science, University of Rochester, Rochester, NY, USA

Soma Mizobuchi
Department of Brain and Cognitive Sciences, University of Rochester, NY, USA
Center for Visual Science, University of Rochester, Rochester, NY, USA

Jie Z. Wang
Department of Brain and Cognitive Sciences, University of Rochester, NY, USA
Center for Visual Science, University of Rochester, Rochester, NY, USA

Michele Rucci
Department of Brain and Cognitive Sciences, University of Rochester, NY, USA
Center for Visual Science, University of Rochester, Rochester, NY, USA

During natural fixation, small eye movements continually modulate the input to the retina. Previous studies have shown that this motion enhances sensitivity to fine spatial detail, a conclusion supported by findings of reduced sensitivity to high—but not low—spatial frequencies when stimuli are immobilized on the retina for brief periods of time. Most prior retinal stabilization studies have relied on fast-phosphor cathode ray tube (CRT) displays or adaptive optics scanning laser ophthalmoscopes (AOSLOs), both of which deliver temporally pulsed stimulation. This raises the question of whether stimulus flicker contributed to the previously observed perceptual impairments under retinal stabilization. Here, we replicate stabilization experiments using two types of fast displays that provide more continuous stimulation: liquid-crystal display (LCD) and organic light-emitting diode (OLED) monitors. We again find an impairment in sensitivity to high spatial frequencies under retinal stabilization. Analyses of the retinal input confirm high-quality stabilization within the temporal bandwidth of human vision. These results show that retinal stabilization effects are robust across display technologies and are little affected by the specific dynamics of modern displays.

Introduction

Humans are unaware that their eyes are always in motion, even when attempting to maintain steady gaze. During the brief intervals between rapid gaze shifts (saccades and microsaccades), a meandering, jittery motion—commonly known as ocular drift—continually shifts the image on the retina across many photoreceptors (Kowler, 2011) (Figure 1A). The temporal modulations generated by this fixational motion provide computational advantages for encoding spatial information (Casile & Rucci, 2009; Kuang, Poletti, Victor, & Rucci, 2012; Rucci & Victor, 2015; Wu et al., 2024), and it has long been proposed that these signals contribute to visual processing (Averill & Weymouth, 1925; Marshall & Talbot, 1942; Ahissar & Arieli, 2001; Rucci, Ahissar, & Burr, 2018).

Recent studies using retinal stabilization, a condition in which the stimulus moves together with the eye to remain stationary on the retina, have provided strong support to this idea: Sensitivity to high-spatial-frequency stimuli is selectively impaired when retinal motion is eliminated for brief periods approximating the duration of natural inter saccadic fixation, as

Citation: Li, Y. H., Mizobuchi, S., Wang, J. Z., & Rucci, M. (2026). Perceptual consequences of retinal stabilization with high-frequency non-stroboscopic displays. *Journal of Vision*, *26*(7):17, 1–13, https://doi.org/10.1167/jov.26.7.17.

https://doi.org/10.1167/jov.26.7.17 Received February 17, 2026; published July 28, 2026 ISSN 1534-7362

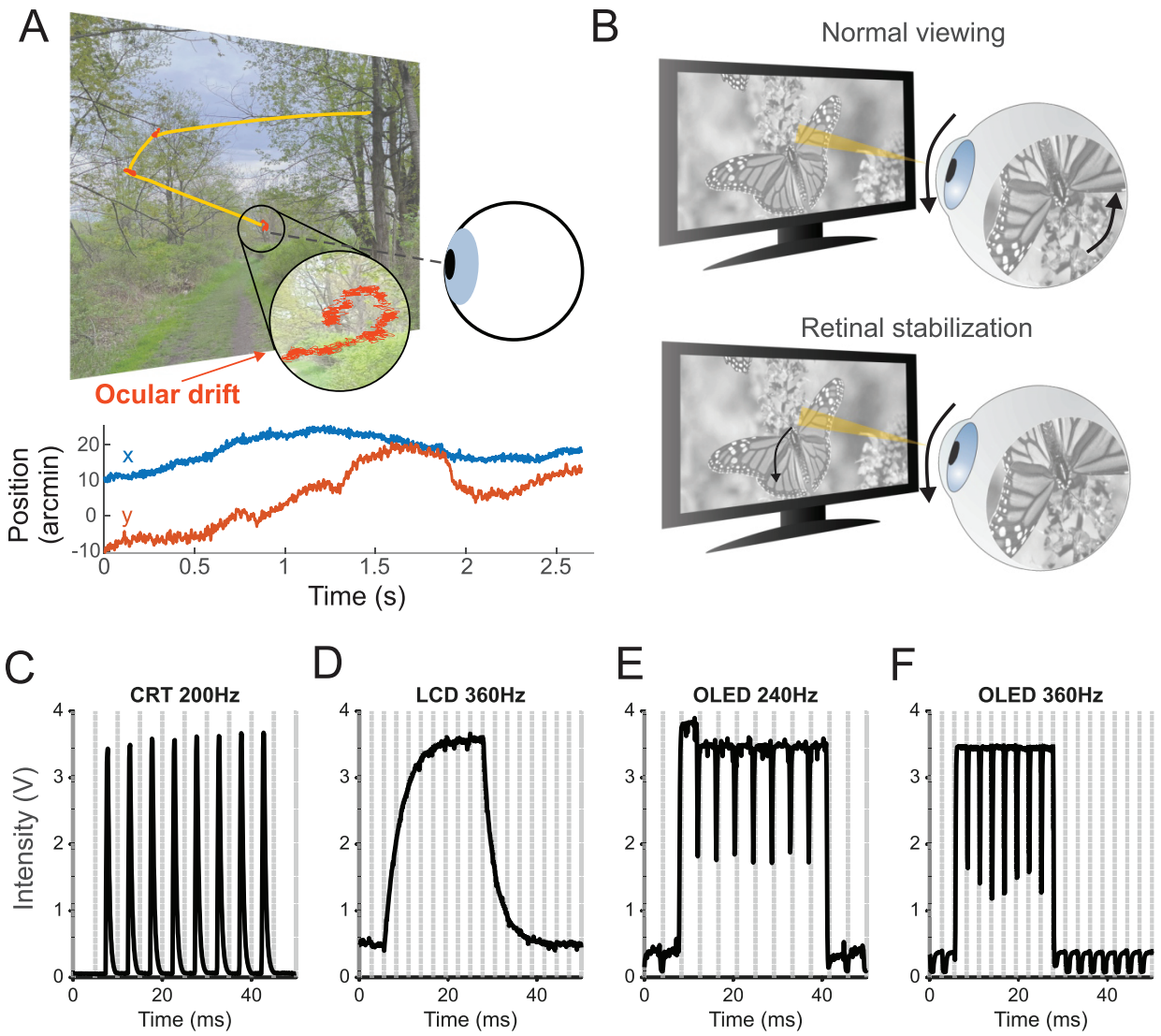

Figure 1. Eye movements, retinal stabilization, and display dynamics. (**A**) An eye movement trace (yellow) superimposed on the observed scene. Naturally occurring ocular drifts during inter saccadic fixations are marked in red. The horizontal and vertical eye positions of the last fixation (zoomed-in inset) are shown in the bottom panel. (**B**) Retinal stabilization procedure. During normal viewing, eye movements cause incessant motion on the retina. Under retinal stabilization, the stimulus moves on the display to counteract the movement of the eye and maintain its projection at a fixed position on the retina. (**C–F**) Refresh dynamics of four types of monitors: a CRT at 200 Hz (**C**), an LCD at 360 Hz (**D**), and two OLEDs at 240 Hz (**E**) and 360 Hz (**F**). Each monitor was driven to display a square gray patch at the center, and luminance was recorded with a photodiode, while the stimulus alternated between black and white every 8 frames (16-frame period). The vertical dashed lines mark the display refresh times.

expected if the visual system makes use of the luminance modulations delivered by fixational drifts (Rucci, Iovin, Poletti, & Santini, 2007; Ratnam, Domdei, Harmening, & Roorda, 2017; Boi, Poletti, Victor, & Rucci, 2017; Intoy & Rucci, 2020; Intoy et al., 2024). In fact, spatial sensitivity closely follows the strength of the fixational modulations in experiments with precisely controlled retinal image motion (Intoy et al., 2024). Furthermore, ocular drifts are modulated in a task-dependent manner consistently with the purposeful use of the resulting spatiotemporal signals (Intoy & Rucci, 2020; Lin, Intoy, Clark, Rucci, & Victor, 2023), and visual acuity varies systematically across individuals according to the characteristics of their ocular drifts (Clark, Intoy, Rucci, & Poletti, 2022).

While a growing body of evidence supports the view that fixational drift contributes to an active strategy for encoding visual information (Rucci & Victor, 2015; Boi et al., 2017), most retinal stabilization experiments have relied on systems that deliver *flickering* stimulation to the retina. For instance, cathode ray tube (CRT) displays render images sequentially, as an electron beam

scans the screen line by line from top to bottom with each frame (Sperling, 1971). Similarly, adaptive optics scanning laser ophthalmoscopes (AOSLOs) generate retinal stimuli by turning a scanning laser on and off, typically at lower refresh rates than CRTs (Ratnam et al., 2017). These presentation methods have raised the question of whether stroboscopic stimulation influenceds the results of retinal stabilization experiments (Gur, 2024).

To address this question, here we replicate previous retinal stabilization experiments using two types of modern displays: liquid-crystal display (LCD) and organic light-emitting diode (OLED) monitors. Both technologies present more continuous stimulation, albeit through different mechanisms (Chen, Lee, Lin, Chen, & Wu, 2018; Hong et al., 2011; Kobayashi, Miyama, Akiyama, Ikemura, & Kitamura, 2022). LCDs eliminate inter frame blanks by employing a constant backlight and updating the voltages applied to the liquid crystals only when the image changes. OLEDs, in contrast, use self-emissive pixels that can be individually and rapidly updated with new image data, enabling near-instantaneous pixel refresh while maintaining constant illumination throughout each frame. For both display types, growing demand for high-performance graphics has led to the development of monitors with high refresh rates, which can, in principle, be used to precisely control retinal stimulation during eye movements.

Methods

Participants

Ten participants took part in this study (five males and five females; age range: 22–35). Five subjects participated in the OLED 240 Hz experiment (Figure 4C), three in the OLED 360 Hz experiment (Figure 4D), and four in the LCD experiment (Figure 4E), with two participants completing both the OLED 360 Hz and LCD experiments. All participants were emmetropic and were compensated for their participation. With the exception of one author, all participants were naive about the purpose of the experiments. Informed consent was obtained from all participants. The study was conducted in accordance with procedures approved by the University of Rochester Institutional Review Board.

Stimuli and apparatus

In three separate experiments, stimuli were displayed on an LCD monitor at 360 Hz (ASUS PG259QN, Asusteck Computer Inc., Taipei, Taiwan), an OLED monitor at 240 Hz (LG UltraGear, LG Electronics Inc., Seoul, Korea), and an OLED monitor at 360 Hz (Alienware AW2725DF, Alienware Corporation, Miami, Florida, U.S.) in a dimly illuminated room. All three monitors were calibrated to linearize the relationship between input RGB values and output luminance. Stimuli consisted of full-field sinusoidal gratings (24° × 15° for the LCD; 41° × 24° for the OLEDs) at high spatial frequency (16 cycles/deg on the LCD; 10 cycles/deg on the OLEDs), tilted by ±45° relative to the horizontal meridian and displayed over a uniform background.

To minimize retinal luminance transients not caused by eye movements, the stimulus contrast ramped up linearly before reaching an individually selected plateau value (Figure 4B). Stimuli were either displayed at a fixed location on the monitor (normal viewing condition) or moved on the display to counteract the motion of the eye (retinal stabilization condition). To assess the consequences of retinal stabilization at distinct retinal eccentricities and also minimize the possibility that the observer would attempt to pursue the stabilized stimulus, thereby altering eye movements between the two conditions, central vision was occluded by an artificial scotoma: a circular opaque gray region with a radius of 1° in the LCD experiment and 7.5° in the OLED experiments surrounded by a 0.5° annulus of tapered transparency, which remained centered on the line of sight as the eyes moved normally during fixation.

As in previous studies (Intoy & Rucci, 2020), stimuli were viewed monocularly with the right eye while the left eye was patched. The participant's head was immobilized by a dental imprint bite-bar and a headrest to maintain a fixed distance from the monitor (123 cm from the LCD and 78 cm from the OLEDs). Movements of the viewing eye were measured with a custom digital Dual Purkinje Image (DPI) eye tracker (Crane & Steele, 1985), a system with demonstrated sub-arcminute resolution (Wu et al., 2023). Stimuli were rendered using EyeRIS, a system for gaze-contingent display control that enables real-time synchronization between oculomotor measurements and image updating on the monitor (Santini et al., 2007) (average delay: 1.5 frames).

Psychophysical procedures and data analysis

Data were collected in several experimental sessions, each lasting approximately 1 hour. Each session was composed of several 10- to 15-minute blocks of trials, separated by breaks to allow participants to rest. Every session began with a two-step calibration procedure to ensure optimal eye tracking and gaze-contingent control, as described previously (Poletti & Rucci, 2016). In this procedure, the spatial registration between eye movements and the stimulus on the monitor was refined in a gaze-contingent phase in which the observer man-

ually corrected possible offsets in the estimated position of gaze, shown in real time as a marker on the display.

The calibration was followed by blocks of experimental trials, in which participants reported whether the grating was tilted to the left or the right. Each trial started with the observer fixating on a central marker (a 10′ dot). After stable fixation was detected, the trial sequence described in Figure 4B was initiated, with the contrast of the stimulus first ramping up for 800 ms and then remaining constant for 500 ms at a contrast value individually selected to yield ∼85% correct responses in the normal viewing condition. A full-field Brownian noise mask ended the trial and prompted the observer to report the perceived orientation of the grating by pressing a corresponding button on a joypad. Both the orientation of the stimulus and the viewing condition—normal viewing (stimulus stationary on the monitor) or retinal stabilization (stimulus stabilized on the retina)—were randomly interleaved across trials.

The sampled oculomotor traces were segmented into periods of saccades and drifts based on an instantaneous speed threshold of 2°/s, as in our previous studies. Performance (reported as d' in Figures 4C–E) was evaluated on the trials in which the eye moved exclusively because of ocular drift during stimulus presentation. All trials containing blinks, saccades, or microsaccades were discarded, as these movements introduce additional luminance transients that are outside the scope of this study. On average, 36% of the trials were discarded. After trial exclusion, an average of approximately 155 valid trials per participant were analyzed in the OLED 240 Hz experiment, 164 in the OLED 360 Hz experiment, and 123 in the LCD 360 Hz experiment.

Retinal stabilization assessment

Retinal stabilization quality was assessed by quantifying the residual retinal image motion and the resulting luminance fluctuations on the retina for each display technology. Using photometric measurements of each monitor's temporal response (Figure 1), we modeled the luminance signal experienced by a simulated photoreceptor during fixation and under retinal stabilization (Figure 2).

Monitor dynamics were measured by displaying temporally modulated gray patches at the center of each monitor and acquiring the resulting luminance signals using a photodiode. For all monitors, contrast and brightness were both set to 50%, with all other settings left at factory defaults. The luminance of the patch was modulated as a square wave with a duty cycle of 50% and a period of 16 frames, an interval long enough to enable the LCD—the monitor with the slowest dynamics—to reach steady state within each half-period. The modulation was set to 50% Michelson contrast and rendered using EyeRIS (Santini et al., 2007). The photodiode (Vishay Intertechnology Inc., Malvern, Pennsylvania, U.S.) was placed 1 cm from the display surface over the patch with a custom enclosure to limit light leakage outside the 25.4-mm × 25.4-mm region. The photocurrent was first converted into voltage by a high-bandwidth transimpedance amplifier, with gain values tuned for each monitor to maintain the output signal within the [0–5] V range. Analog voltages were then sampled at 10 kHz and quantized to 16 bits via a PCIe ADC board (General Standards Corporation, Huntsville, Alabama, U.S.), yielding traces like those reported in Figures 1C–F.

Based on the recorded luminance traces, we modeled each monitor's dynamics to derive temporal filters that simulated the output luminance $\widehat{L}(t)$ given a time-series of requested luminance values:

$$L_{\text{cmd}}(t) = L(nT) \quad \text{for} \quad t \in [nT, (n+1)T), \quad n \in \mathbb{Z}, \quad (1)$$

where $L(nT)$ is the desired luminance value at each frame (T is the frame interval, i.e., the inverse of the refresh rate). For all monitors, luminance traces were modeled at 10 kHz ($\Delta t = 100$ µs) to match the sampling rate at which data were acquired.

The output of the CRT was estimated as

$$\widehat{L}(t) = \sum_{n=-\infty}^{\infty} L_{\text{cmd}}(nT)\, h(t - nT; \alpha, \lambda) \quad (2)$$

where T was 5 ms and $h(t; \alpha, \lambda)$ is a causal gamma-shaped kernel fitted to model the CRT pulses:

$$h(t; \alpha, \lambda) = A \frac{\lambda^{\alpha}}{\Gamma(\alpha)} t^{\alpha-1} e^{-\lambda t} \quad \Gamma(\alpha) = \int_0^{\infty} t^{\alpha-1} e^{-t} dt \quad (3)$$

The parameters $\alpha = 3.196$ and $\lambda = 4.8\,\text{ms}^{-1}$ were estimated to fit the photodiode measurements, and A was set to ensure that the kernel reached unit value at its peak ($t_p = \frac{\alpha-1}{\lambda}$), that is, $A = \left[\frac{\lambda^{\alpha}}{\Gamma(\alpha)} t_p^{\alpha-1} e^{-\lambda t_p}\right]^{-1}$. Because the CRT emits light in brief pulses rather than sustained intervals, the simulated CRT output was scaled so that its time-averaged luminance matched the requested luminance. Equivalently, the CRT pulse train was normalized by its temporal integral, ensuring that CRT and non-stroboscopic displays delivered comparable total light over time. This scaling results in higher instantaneous luminance during each CRT pulse, while preserving comparable mean luminance across display types.

The dynamics of the LCD and OLED monitors were modeled with a first-order difference equation:

$$\widehat{L}(t) = \widehat{L}(t - \Delta t) + \left(L(t) - \widehat{L}(t - \Delta t)\right)\left(1 - e^{-\Delta t/\tau}\right), \quad (4)$$

where $L(t)$ was set equal to $L_{\text{cmd}}(t)$ in Equation 1 for the LCD and equal to L_{OLED} in Equation 5 below for

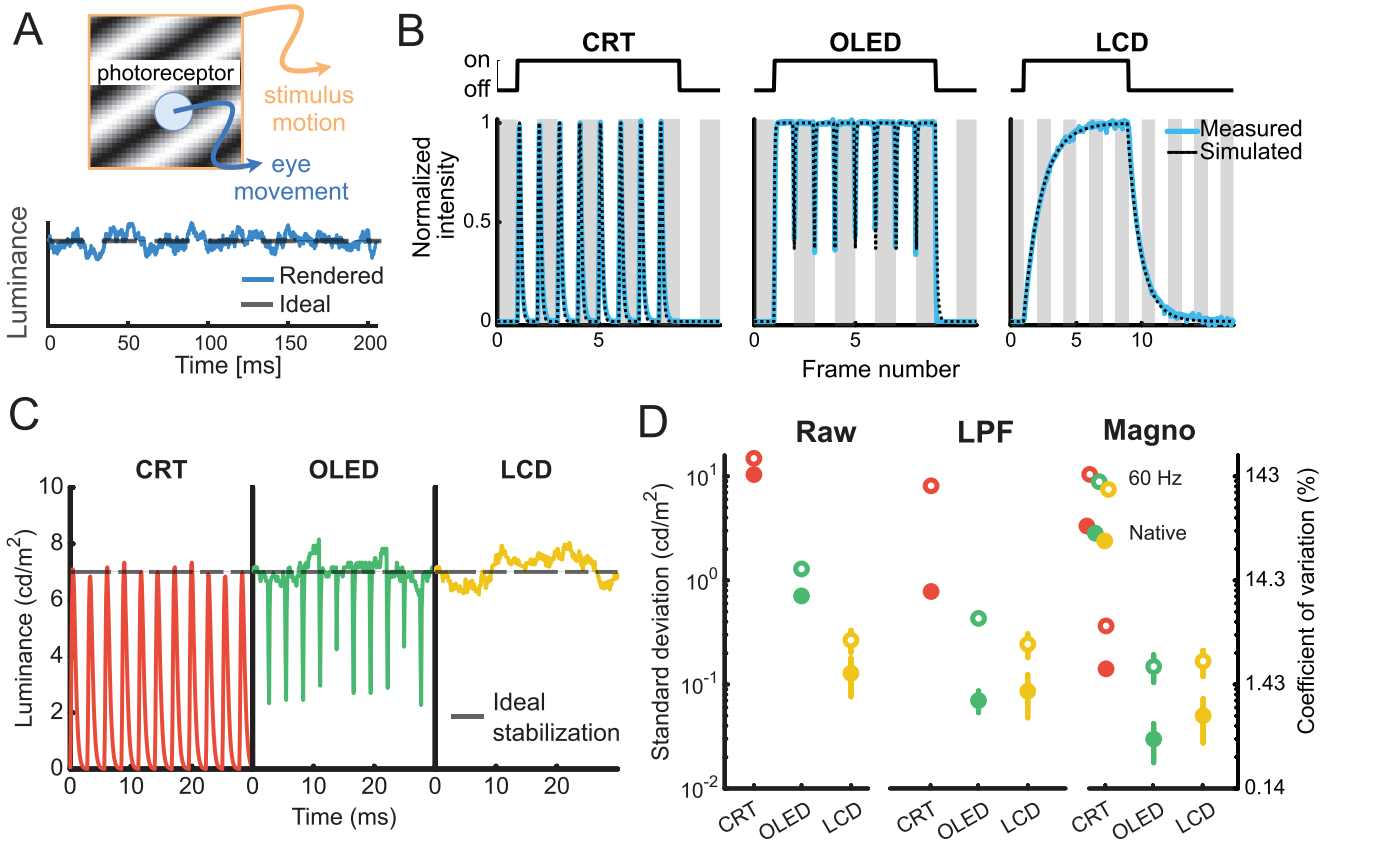

Figure 2. Impact of display refresh dynamics on retinal stabilization. (**A**) Ideally, compensating for the observer's eye movements (blue trace) by continually updating the stimulus on the monitor (orange trace) should produce a constant visual input at the level of individual photoreceptors (bottom panel; dashed line). In practice, however, even with perfect oculomotor measurements, the temporal dynamics of the display introduce fluctuations in the input signal (bottom panel; blue trace). (**B**) Modeling monitor dynamics. The temporal characteristics of three monitors were modeled based on the luminance measurements obtained while driving each monitor with a 16-frame square wave. Monitors were driven at their maximum refresh rates: 200 Hz for the CRT (left), 360 Hz for the OLED (middle), and 360 Hz for the LCD (right). For each monitor, the simulated intensity values (dashed black lines) are compared with the luminance measurements (solid blue lines). (**C**) Simulated retinal input during gaze-stabilized fixations. The gray dashed line represents ideal stabilization, in which the retinal input remains constant. Colored lines show the modeled luminance signals experienced under retinal stabilization with the CRT (left, red), the OLED (middle, green), and the LCD (right, yellow). (**D**) Estimated variability in the retinally stabilized input stimulation provided by the three monitors. Data points represent the standard deviation (left ordinate) and corresponding coefficient of variation (right ordinate) for the raw input signals (left panel), after low-pass filtering at 80 Hz (center panel), and after filtering by the temporal sensitivity of magnocellular ganglion cells (right panel). Results are shown for each monitor at its maximum refresh rate (filled markers) and at 60 Hz (open markers). Error bars represent ± 1 standard deviation across 20 simulated retinal locations and 50 fixations.

the OLED monitor. Two different time constants, τ_{rise} and τ_{fall}, were used for increments or decrements in intensity, respectively. Time constants were obtained by fitting the luminance traces recorded from each monitor, excluding the brief inter frame luminance dips observed in the OLED traces immediately before each new frame. Estimated parameters were $\tau_{\text{rise}} = 3.7$ ms and $\tau_{\text{fall}} = 2.8$ ms for the LCD and $\tau_{\text{rise}} = 0.08$ ms and $\tau_{\text{fall}} = 0.2$ ms for the OLED.

To model the OLED intraframe blanking, the commanded luminance input in Equation 4 was multiplied by a periodic gating function that shut down pixel drive for a fraction of each frame period T. That is,

$$L_{\text{OLED}}(t) = L_{\text{cmd}}(t)\, p(t) \quad (5)$$

where

$$p(t) = \sum_{n=0}^{\infty} P(t - nT), \qquad P(t) = \begin{cases} 1 & 0 \le t < \tau_{\text{ON}} \\ 0 & \text{otherwise.} \end{cases}$$

Here, $\tau_{\text{ON}} = 2.6$ ms was estimated by fitting the model to the measured luminance dynamics from the OLED monitor.

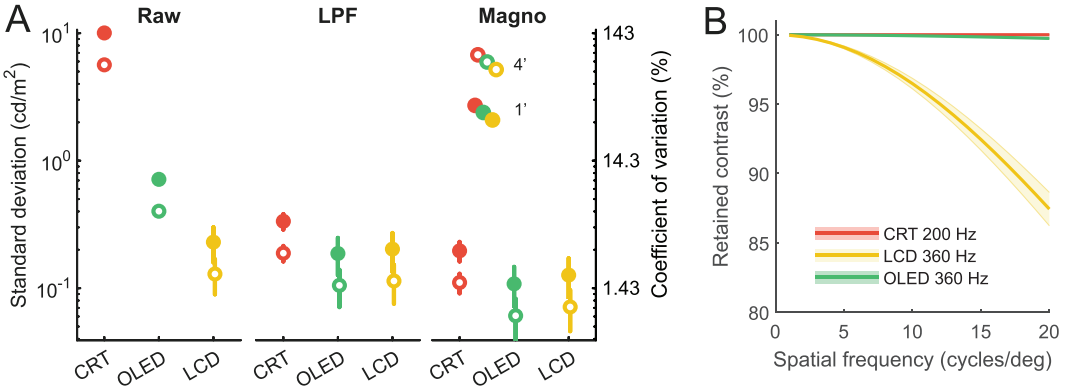

Figure 3. Additional factors affecting gaze-contingent rendering. (**A**) Stabilization errors after incorporating additional practical limitations beyond monitor dynamics. These simulations included the measured rendering delay of our gaze-contingent system and different diameters of the retinal sampling aperture. Filled markers represent smaller apertures, and open markers represent larger apertures. Other conventions are the same as in Figure 2D. (**B**) Effect of display dynamics on the effective contrast of stabilized gratings. Monitors with slower pixel dynamics can attenuate the physical contrast of a stabilized stimulus, because pixels may not fully reach their intended luminance values before the next gaze-contingent update. This effect depends on the spatial frequency of the stimulus and is most pronounced for the LCD monitor (yellow).

Retinal stabilization errors were estimated by modeling the luminance fluctuations that would be experienced at individual retinal locations (Figures 2C, 2D) or by photoreceptors with finite sampling apertures (Figure 3A) as a consequence of the measured display dynamics and gaze-contingent updating procedures. Specifically, ocular drift was modeled as a Brownian motion process with diffusion constant $D = 20$ arcmin^2/s, a value representative of drift measured during high-acuity fixation tasks. Oculomotor traces were generated at 10 kHz to match the time step of the temporal filters in Equations 1–4. They were then resampled at 1 kHz to match the eye-tracking sampling rate and quantized into display pixel coordinates (1 pixel = 10′).

For each monitor, we modeled the luminance experienced by an array of 20 retinal samples evenly spaced over one period of the grating, as the eye drifted for 500 ms. In Figure 2, the sampling aperture was restricted to the simulated monitor resolution (10′) to provide a conservative upper-bound estimate of the stabilization error. Figure 3A shows results for larger retinal sampling apertures corresponding to different photoreceptors. We quantified the degree to which retinal input deviates from ideal stabilization by computing the standard deviation and corresponding coefficient of variation of the simulated raw luminance signals as well as of the signals filtered by two perceptually motivated temporal filters: a fourth-order Butterworth IIR low-pass filter with an 80 Hz cutoff frequency, a conservative upper limit for human achromatic flicker fusion (Hecht & Shlaer, 1936; De Lange Dzn, 1954), and a filter simulating the responses of macaque magnocellular retinal ganglion cells (Victor, 1987):

$$H_M(\omega) = Ae^{-\imath\omega D_M}\left(1 - \frac{H_S}{1+\imath\omega\tau_S}\right)\left(\frac{1}{1+\imath\omega\tau_L}\right)^{N_L}$$

$$\tau_S(c) = \frac{T_0}{1+\left(\frac{c}{C_{1/2}}\right)^2}$$

This model was originally developed for cat X cells and later shown to predict the responses of macaque P and M cells when parameters are appropriately tuned (Benardete & Kaplan, 1997, Benardete & Kaplan,1999). Parameters were taken from the neurophysiological literature to model the responses of cells located at approximately 5° eccentricity (Benardete & Kaplan, 1999): $N_L = 30.3$, $A = 499.77$ impulses · s^{-1}, $D_M = 2.0$ ms, $H_S = 1.00$, $\tau_L = 1.44$ ms, $T_0 = 37.34$ ms, $C_{1/2} = 0.051$, and $c = 0.50$. The data in Figure 2D reflect averages across 1,000 simulated luminance traces (20 photoreceptors × 50 fixations) per monitor.

The simulations in Figure 3 also incorporated system delays beyond monitor dynamics, including the 1-ms sampling delay of the dDPI eye tracker (Wu et al., 2023) and the delay of the gaze-contingent display control system used in the experiments shown in Figure 4 (Santini et al., 2007). The latter delay reflects the sum of the fixed one-frame delay introduced by the processing pipeline and the additional delay associated with raster rendering on the display. For a stimulus located near the center of the screen, this raster-rendering component corresponds to approximately half a frame, yielding an average total delay of ∼1.5 frames.

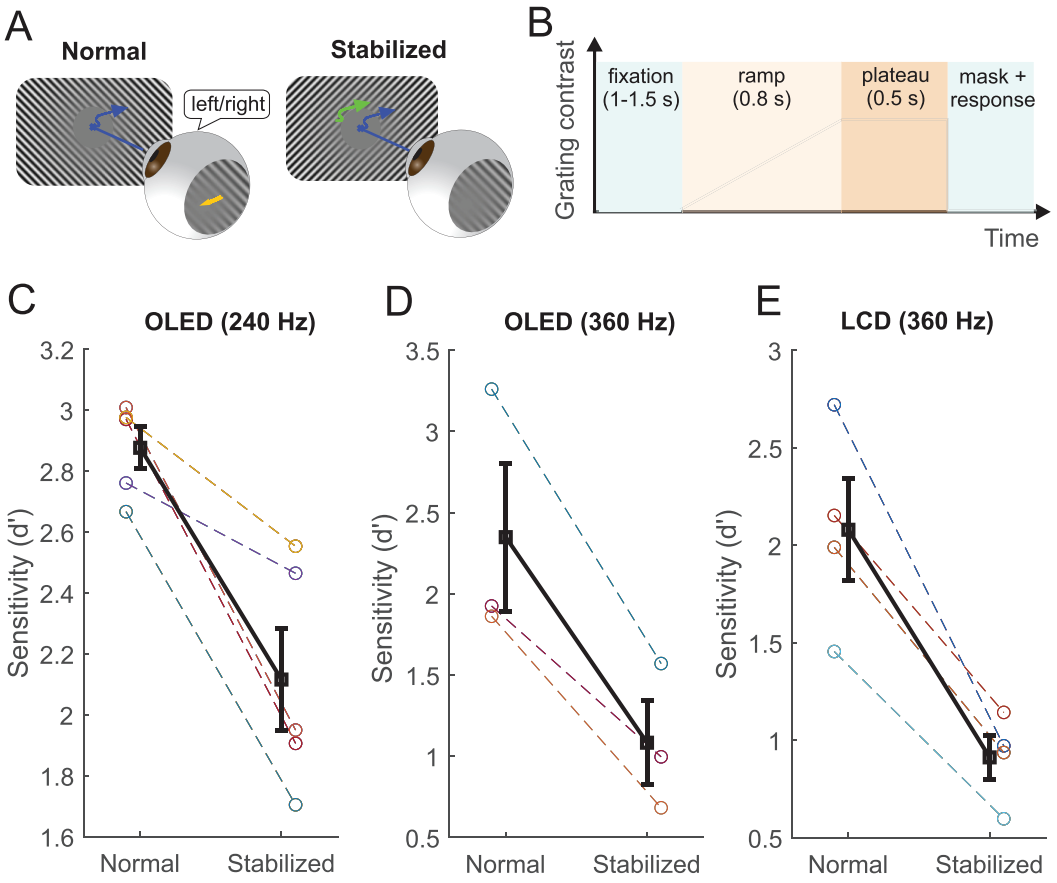

Figure 4. Perceptual consequences of retinal stabilization. (**A**) A high-frequency orientation discrimination task under normal viewing (left) or retinal stabilization (right). (**B**) The temporal sequence of a trial. Stimulus contrast ramped up for 0.8 s, followed by a 0.5-s plateau period. A full-screen noise mask ended the trial. (**C–E**) Measured sensitivity (expressed as *d'*) when stimuli were rendered on three different monitors: (**C**) OLED monitor at 240 Hz. Stabilizing the stimulus on the retina impairs sensitivity for all subjects ($N = 5$; $p = 0.01$, paired *t*-test). (**D**) OLED monitor at 360 Hz ($N = 3$; $p = 0.03$, paired *t*-test). (**E**) LCD monitor at 360 Hz ($N = 4$; $p = 0.01$, paired *t*-test). In all panels, thin lines indicate individual subjects, and the black line shows the average ± SEM across subjects. Across all display types, retinal stabilization reduced sensitivity for high-frequency orientation discrimination.

Results

In retinal stabilization experiments, the position of the stimulus is updated at each refresh of the display to compensate for the observer's eye movements, thereby keeping the stimulus stationary on the retina (Figure 1B). To minimize errors caused by fast eye movements, this procedure is typically restricted to periods of relatively slow intersaccadic fixation, while trials containing saccades or microsaccades are excluded from analysis (Intoy et al., 2024). In this study, we first evaluate the quality of retinal stabilization resulting from distinct display technologies. We then present psychophysical measurements obtained using different monitors to examine possible influences of display dynamics.

Quality of retinal stabilization

Figures 1C–F illustrates the temporal luminance dynamics of four displays—a CRT, an LCD, and two OLED monitors—when displaying a uniform 25-mm × 25-mm square patch. The luminance signals were recorded using a photodiode (Vishay Intertechnology Inc.) while the patch alternated between black and white in a square-wave modulation with a 16-frame period. Each display was tested at its maximum refresh rate: 200 Hz for the CRT, 360 Hz for the LCD, and 240 Hz and 360 Hz for the two OLEDs, respectively.

As expected, the CRT monitor exhibits the stereotypical stroboscopic pattern, with brief luminance spikes occurring at every passage of the beam interleaved by long blank periods as the phosphors decay (Figure 1C). In contrast, the LCD monitor gives

a smoother temporal profile, with gradual increases and decreases in luminance and no interruptions in visual stimulation (Figure 1D). The two OLED monitors (Figures 1E, 1F) are characterized by fast response times and steady luminance levels, except for very brief transient dips in intensity immediately before each refresh of the image due to so-called inter frame blanking, a common feature of OLED monitors. Unlike the CRT, however, these interruptions have extremely short durations, lasting less than 0.5 ms.

To estimate the quality of retinal stabilization afforded by each monitor, we modeled the changes in luminance that a retinal photoreceptor would experience in a typical experiment (Figure 2A). Based on the photodiode measurements, we derived temporal filters that captured the persistence and temporal response of each monitor. Specifically, we used a gamma kernel to model the luminance spikes of the CRT monitor and first-order low-pass filters with separate time constants for luminance increments and decrements for the LCD and OLED displays, and we tuned the respective parameters to closely fit the recorded luminance data (Figure 2B). We modeled fixational eye drift as a Brownian motion process with diffusion constant $D = 20$ arcmin^2/s, a model that well replicates the characteristics of inter saccadic eye movements (Desbordes & Rucci, 2007; Engbert, Mergenthaler, Sinn, & Pikovsky, 2011; Rucci & Poletti, 2015). As in previous retinal stabilization experiments with stimuli at high spatial frequencies (Rucci et al., 2007; Boi et al., 2017) and the experiments described later in this article, we assumed the stimulus to be a 10 cycles/deg grating.

Under perfect stabilization, the input signal experienced by a photoreceptor would remain constant over time (dashed lines in Figures 2A, 2C), as the stimulus would move to counteract the consequences of eye movements. In practice, however, luminance varies because of the characteristics of each display, which result in temporal fluctuations in the input signal (colored lines in Figure 2C). These modulations differ across display types: They contain gradual changes when the stimulus is displayed on the LCD (yellow trace in Figure 2C), brief luminance pulses for the CRT (red trace), and extremely brief interruptions in visual stimulation for the OLEDs (green trace).

We evaluated the precision of retinal stabilization by calculating how much the luminance input to any given retinal location deviates from the ideal case of constant stimulation (Figure 2D). As expected, when looking at the raw input data, the luminance pulses introduced by stroboscopic displays, such as CRTs, cause large deviations from the intended values. The other monitors did not exhibit the large deviations present in the CRT because of their more sustained responses. This was particularly evident for the LCD, which delivers almost constant stimulation once it reaches its steady state.

To quantify the quality of retinal stabilization, the left panel of Figure 2D shows the standard deviation (left ordinate) and the corresponding coefficient of variation (the percentage deviation from the mean, right ordinate) experienced by the modeled photoreceptor in a typical trial of a retinal stabilization experiment for the three types of monitors. In terms of the full (unfiltered) luminance signals, the LCD monitor yields the smallest variability, with about a 1.8% change in luminance during the course of an experimental trial.

It is important to emphasize that these raw data, reported in the left panel of Figure 2D, provide an overestimation of the effective error in retinal stabilization. These data consider all fluctuations in the input signal at all temporal frequencies, irrespective of whether they are within or outside of the temporal sensitivity bandwidth of the visual system. For example, much of the deviation in the CRT occurs at frequencies well beyond the visual system's sensitivity. To elucidate this, consider an ideal CRT display that instantaneously updates phosphors with zero persistence. In this case, the input stimulus would be a train of flashes separated by the refresh interval (in our case, 5 ms, since the monitor was updated at 200 Hz), which in the frequency domain would correspond to a stack of harmonics at integer multiples of the display frequency. Only the DC (0 Hz) component of this stimulus would be detected by the visual system (corresponding to our percept of an unflickering monitor), because all the other harmonics are well beyond what can be resolved by the visual system. Considering very high frequency harmonics leads to an inflated estimation of the perceptual impact of the stabilization error.

To estimate the perceptually relevant consequences of imperfect stabilization, we examined the stabilization error after filtering the input signals according to the temporal sensitivity of human vision. The data in the center and right panels of Figure 2D quantify the fluctuations in luminance experienced at a fixed retinal location after applying two perceptually relevant filters: a low-pass filter with an 80 Hz cutoff frequency, a conservative upper limit for flicker fusion (Hecht & Shlaer, 1936; De Lange Dzn, 1954) (Figure 2D, center panel), and a filter designed to replicate the temporal response of macaque magnocellular retinal ganglion cells—the retinal neurons most sensitive to higher temporal frequencies—as measured in neurophysiological recordings (Benardete & Kaplan, 1999) (Figure 2D, right panel). Both analyses show that all monitors provide high-quality retinal stabilization within the relevant temporal bandwidth. This includes CRTs operated at high refresh rates, because although these displays deliver stroboscopic stimulation, the resulting luminance fluctuations occur largely outside the range relevant for perception and early neural responses. Critically, the quality of retinal stabilization

deteriorates when display updates occur less frequently (Figure 2D).

Figure 2D reports the stabilization errors attributable solely to monitor dynamics. For completeness, we also simulated the effects of additional factors that can influence the quality of retinal stabilization, including delays in the eye-tracking/rendering pipeline and the spatial extent of photoreceptor sampling on the retina. Figure 3A shows the resulting errors after incorporating the measured delay of the gaze-contingent apparatus used in the experiments described later in this study (Santini, Redner, Iovin, & Rucci, 2007), as well as the impact of sampling the stimulus with photoreceptors of different aperture sizes (Watson, 2014). As shown by these simulations, the rendering delay had a minimal impact compared with the effects of monitor dynamics alone (compare Figure 3A with Figure 2D). In contrast, increasing cone aperture reduced the estimated stabilization error, because larger apertures are less sensitive to small residual image displacements. For example, increasing the diameter of the sampling aperture from 1 to 4 arcmin reduced the error by 43.8%, illustrating how broader spatial integration reduces sensitivity to small residual stabilization errors.

The analysis in Figure 2D quantifies deviations from ideal stabilization at a single retinal location, but it does not address a separate question: whether the effective contrast of the stimulus is preserved when the image is shifted on the display to compensate for eye movements. This concern is particularly relevant for monitors with relatively slow rise and fall times. If a pixel's luminance lags behind the requested value, it may fail to reach its intended level before the next gaze-contingent update, thereby attenuating the effective contrast of the stabilized image. As shown by our simulations in Figure 3B, the magnitude of this attenuation depends on the spatial frequency of the stimulus. For a grating at 16 cycles/deg, the 360 Hz LCD produced an approximately 8% reduction in contrast, whereas the faster OLED display produced only a minimal change. Thus, monitors with slower temporal dynamics, such as the LCD tested here, can provide accurate retinal stabilization while introducing a small attenuation of the effective contrast at high spatial frequencies.

Perceptual consequences of retinal stabilization

Having established that all three monitors yield high-quality retinal stabilization, we examined whether eliminating retinal motion for durations comparable to natural intersaccadic fixation impairs fine-pattern discrimination when stimuli are rendered on OLED and LCD displays, as previously reported with CRT displays.

The experimental procedure was similar to our previous experiments with retinal stabilization (Rucci et al., 2007; Boi et al., 2017; Intoy et al., 2024). In a binary classification task, subjects were asked to report whether a high-frequency grating was tilted by 45° to the left or to the right (Figure 4A). Each trial started with the observer fixating on a marker at the center of a uniform gray field. To minimize luminance transients caused by stimulus presentation, the stimulus then appeared gradually with contrast increasing linearly over an initial period of 800 ms, followed by a 500-ms exposure at plateau contrast. The orientation of the grating varied randomly across trials. A large-field maximum-contrast noise mask ended the trial, prompting subjects to report the perceived orientation of the grating by pressing one of two buttons on a joypad (Figure 4B).

Trials randomly alternated between two conditions: normal viewing and retinal stabilization. In both conditions, eye movements were continually recorded by means of a high-resolution dual Purkinje Image eye tracker (Wu et al., 2023), a system that provides arcminute resolution with a ∼1-ms delay. Following the approach used in our previous studies, stabilization was achieved by means of a custom system for gaze-contingent display control (Santini et al., 2007). This approach has been shown to achieve high-quality retinal stabilization with errors of the order of 1 arcminute (Rucci et al., 2007) (see Figure 3A). As customary in retinal stabilization experiments, to isolate the influence of the luminance modulations resulting from ocular drift, all trials containing blinks, saccades, or microsaccades during stimulus presentation were excluded from the analysis. In separate experimental sessions, distinct groups of subjects were exposed to stimuli rendered on one of the three monitors, an LCD and an OLED driven at 360 Hz, both modeled in Figure 2, and an OLED driven at 240 Hz (Figure 1E).

As shown in Figures 4C–E, retinal stabilization substantially impaired fine-pattern discrimination, irrespective of the display used to render the stimuli. Similar decrements in performance were measured with the 240 Hz OLED ($N = 5$; $p = 0.01$, paired t-test; Figure 4C), the 360 Hz OLED ($N = 3$; $p = 0.03$; Figure 4D), and the LCD monitor ($N = 4$; $p = 0.01$; Figure 4E). On average across subjects, sensitivity decreased by 43%, an impairment consistent with previous observations obtained using CRT displays at a lower (200 Hz) refresh rate (Rucci et al., 2007; Intoy & Rucci, 2020). The reduction was consistent across observers, with every participant showing lower performance under stabilization. These data show that the perceptual impairments previously reported under brief periods of retinal stabilization are robust with respect to display technology and refresh rate. Perception of high spatial frequency patterns is

impaired in the absence of the visual input changes normally resulting from eye movements.

Discussion

During natural fixation, the eye moves incessantly, continually translating the image on the retina and transforming a static scene into temporal luminance modulations at the level of individual photoreceptors. A growing body of work indicates that these luminance modulations contribute to spatial vision, particularly for fine detail. Notably, discrimination of fine patterns and sensitivity to high spatial frequencies, but not low spatial frequencies, are impaired when retinal motion is eliminated for brief intervals comparable to inter saccadic fixation (Rucci et al., 2007; Ratnam et al., 2017; Intoy & Rucci, 2020). The present study extends these findings by testing a methodological concern: whether perceptual impairments reported under retinal stabilization could be attributed to the stroboscopic nature of the displays traditionally used to implement gaze-contingent stimulation, such as CRTs and adaptive optics scanning laser systems. Using high-refresh LCD and OLED monitors that provide more continuous stimulation, we again observed a robust reduction in sensitivity to high spatial frequencies when retinal image motion was removed. Thus, the perceptual impairment observed under retinal stabilization cannot be explained by the stroboscopic temporal structure of traditional display systems. Instead, these results provide further support for the idea that the deficit arises from the elimination of the luminance modulations normally produced by eye movements, reinforcing the conclusion that these modulations play a functional role in fine spatial vision.

The impairment in sensitivity observed in this study, approximately 43% on average, is comparable in magnitude to previous reports from retinal stabilization studies (Rucci et al., 2007; Ratnam et al., 2017; Boi et al., 2017; Intoy & Rucci, 2020; Intoy et al., 2024). Intoy and Rucci (2020) reported a 40% reduction in acuity, and Boi et al. (2017) observed a similar drop in contrast sensitivity at 10 cycles/deg. More recently, Intoy et al. (2024) reported a 34% reduction at 16 cycles/deg under full retinal stabilization. Rucci et al. (2007) measured the full contrast sensitivity function in two observers and reported sensitivity losses at high spatial frequencies of approximately 25%–35%, depending on spatial frequency. These numbers may, however, underestimate the consequences of stabilization because, unlike the other studies considered here, the stabilized condition in Rucci et al. (2007) also included the normal transients generated by saccades, which are known to influence perception (Boi et al., 2017). In Ratnam et al. (2017), performance was reported in percent correct and decreased by approximately 23% under retinal stabilization. Thus, despite differences in task, stimulus conditions, and measurement scale, the present results fall toward the upper end of the range of previous reports, further arguing against the possibility that stroboscopic stimulation was a significant contributor to the impairments reported previously under retinal stabilization.

Our analyses considered both photometric measurements of display dynamics (Figure 1) and simulations of photoreceptor exposure under retinal stabilization (Figures 2 and 3). Although CRT, LCD, and OLED monitors can provide comparable perceived image quality, their physical luminance time courses differ markedly. In CRTs, stabilization errors computed from unfiltered luminance signals are dominated by high-frequency components generated by stroboscopic rendering, which fall largely outside the temporal bandwidth of visual perception. Thus, assessing retinal stabilization quality directly from raw signals overestimates stabilization errors by incorporating temporal fluctuations that are not perceptually relevant. When the input signals are analyzed within the temporal bandwidth of visual perception and early retinal responses, the dark periods following CRT phosphor decay contribute little to the stabilization error. As a consequence, the effective quality of retinal stabilization with CRTs is comparable to that obtained with more continuous displays, such as LCD and OLED monitors, despite their different temporal dynamics.

High refresh rates further limit residual imperfections in gaze-contingent rendering by reducing the retinal displacement that can accumulate between stimulus updates. For example, with a typical drift speed of ∼30 arcmin/s and a 360 Hz update rate, the eye moves only ∼5 arcsec between refreshes—about 1.4% of the period of a 10-cycle/deg grating, corresponding to an average luminance change of ∼5.5% of the modulation amplitude. Any slower drift would reduce this bound proportionally. Our simulations further show that the additional delay introduced by a properly designed gaze-contingent processing pipeline has relatively little impact on stabilization quality (Figure 3A). Thus, under the refresh rates and response dynamics tested here, the effective departures from ideal stabilization are minimal in the perceptually relevant domain. Displays with slower response times or lower refresh rates would be expected to yield larger residual modulations, as illustrated by the 60 Hz simulations in Figure 2D, and should therefore be evaluated using similar methods when designing retinal stabilization experiments.

While our analyses show that even high-refresh displays with relatively slow pixel dynamics, such as the LCD monitor tested here, can provide high-quality retinal stabilization, the contrast of the stabilized stimulus can be attenuated relative to a normal, unstabilized presentation. The magnitude of this attenuation depends on the spatial frequency of the

stimulus. At 16 cycles/deg, the high spatial frequency used in the LCD experiment, the stabilized grating retained approximately 92% of the contrast of the same grating rendered stationary on the display. This 8% contrast attenuation may have contributed to the large ∼56% behavioral impairment measured in the LCD experiment. It is, however, unlikely to have accounted for the entire effect, as doing so would require an unusually steep psychometric function over a narrow contrast range. Furthermore, the same analysis showed that contrast attenuation was negligible for the OLED monitors, and the OLED experiments also yielded robust perceptual impairments under retinal stabilization (∼37%–40% on average; Figure 4). Thus, LCD dynamics may have contributed to the measured impairment, but they cannot plausibly account for the full perceptual effect.

The reduction in performance measured when high spatial frequency stimuli are examined during brief periods of retinal stabilization suggests that eliminating the temporal luminance modulations normally resulting from ocular drifts impairs fine pattern vision. Neurons in the visual system are known to be highly sensitive to temporal changes (Derrington & Lennie, 1984; Purpura, Tranchina, Kaplan, & Shapley, 1990; Kaplan & Benardete, 2001). Although this preference for non zero temporal frequencies is typically examined with respect to the motion of objects in the scene, neurons are always exposed to temporal changes on the retina, as the self-motion of the observer generates dynamic sensory signals even for stationary objects—that is, it redistributes the power of a static stimulus across nonzero temporal frequencies—offering valuable information about its spatial structure. The idea that the visual system uses temporal modulations to encode spatial patterns dates back more than a century (Averill & Weymouth, 1925; Marshall & Talbot, 1942). Early proposals focused specifically on the limits of visual acuity, but using temporal changes from ocular drifts for encoding fine spatial patterns in general makes sense from a computational perspective, as the power that ocular drift makes available in the form of temporal changes (i.e., the power at non zero temporal frequencies) increases with spatial frequency within a range that, in diffusion models, varies inversely with the drift diffusion constant (Kuang et al., 2012). During viewing of natural scenes, this reformatting counterbalances the power spectrum of natural scenes, yielding an effective visual input that equalizes ("whitens") temporal power over a broad spatial frequency range, an operation that compresses information and has long been proposed as one of the functions of early visual processing (Barlow, 1961; Atick, 1992).

In keeping with this space-time encoding idea, it has been shown not only that eliminating drift-induced motion selectively impairs sensitivity to high spatial frequencies (Rucci et al., 2007; Ratnam et al., 2017) and that individual drift characteristics predict acuity limits (Clark et al., 2022), but also that sensitivity closely follows the strength of the resulting modulations when retinal image motion is experimentally controlled (Intoy et al., 2024). Furthermore, humans adjust drift in a task-dependent manner in ways that enhance these modulations (Intoy & Rucci, 2020; Lin et al., 2023). Importantly, the use of oculomotor-induced temporal transients is not limited to drift. Perceptual enhancement consistent with the spatial information conveyed by movement-generated transients has been reported for smooth pursuits (Yang, Victor, & Rucci, 2025), microsaccades (Mostofi, Boi, & Rucci, 2016), saccades (Li, Cox, Victor, & Rucci, 2025), and even blinks (Yang, Intoy, & Rucci, 2024). Although these behaviors differ markedly in their kinematics, they redistribute stimulus power across temporal frequencies following qualitatively similar profiles, with a progressively narrower whitening band that approaches zero for eye blinks. These results suggest a parsimonious active-encoding strategy in which common neural mechanisms operate on oculomotor-driven luminance transients generated by multiple types of oculomotor activity to support spatial vision. In this view, visual representations depend not only on the spatial pattern on the retina but also on how eye movements structure the incoming flow of luminance signals over time (Kuang et al., 2012; Intoy et al., 2024).

In sum, our study shows that high-refresh CRT, LCD, and OLED displays yield comparable retinal stabilization quality and convergent perceptual consequences. More broadly, we provide a general approach for testing and validating gaze-contingent stimulation on modern display hardware. These findings establish high-refresh LCD/OLED monitors as reliable platforms for psychophysical and neurophysiological studies that probe the consequences of disrupting visuomotor loops via retinal stabilization.

Keywords: fixational eye movements, retinal stabilization, retinal sampling, display technologies

Acknowledgments

The authors thank the members of the Active Perception Laboratory at the University of Rochester for helpful discussions.

Supported by grants R01 EY18363 and P30 EY001319 from the National Institutes of Health.

Author contributions: YHL and MR conceived the study. YHL and JZW implemented the psychophysical

experiments, collected the behavioral data, and analyzed the results. SM collected the monitor measurements and implemented the simulations. All authors contributed to writing the article. MR supervised the project.

Data and code availability: The data and code generated in this study been deposited on Mendeley data (doi:10.17632/f3fygbgvcr.1).

Commercial relationships: MR is an inventor on a patent related to the digital Dual Purkinje Image eye-tracking method used in this study.
Corresponding author: Y. Howard Li.
Email: yli162@u.rochester.edu.
Address: Meliora Hall 258, University of Rochester, Rochester, NY 14623, USA.

References

Ahissar, E., & Arieli, A. (2001). Figuring space by time. *Neuron, 32*, 185–201.

Atick, J. (1992). Could information theory provide an ecological theory of sensory processing? *Network: Computation in Neural Systems, 3*, 213–251.

Averill, H. I., & Weymouth, F. W. (1925). Visual perception and the retinal mosaic. II. The influence of eye movements on the displacement threshold. *Journal of Comparative Psychology, 5*, 147–176.

Barlow, H. B. (1961). Possible principles underlying the transformations of sensory messages. In W. A. Rosen blith (Ed.), *Sensory communication* (pp. 217–234). Cambridge, MA: MIT Press.

Benardete, E. A., & Kaplan, E. (1997). The receptive field of the primate P retinal ganglion cell, I: Linear dynamics. *Visual Neuroscience, 14*, 169–185.

Benardete, E. A., & Kaplan, E. (1999). The dynamics of primate M retinal ganglion cells. *Visual Neuroscience, 16*, 355–368.

Boi, M., Poletti, M., Victor, J. D., & Rucci, M. (2017). Consequences of the oculomotor cycle for the dynamics of perception. *Current Biology, 20*(4), 197–232.

Casile, A., & Rucci, M. (2009). A theory of the influence of eye movements on the refinement of direction selectivity in the cat's primary visual cortex. *Network: Computation in Neural Systems, 20*, 1–13.

Chen, H.-W., Lee, J.-H., Lin, B.-Y., Chen, S., & Wu, S.-T. (2018). Liquid crystal display and organic light- emitting diode display: Present status and future perspectives. *Light: Science & Applications, 7*, 17168.

Clark, A. M., Intoy, J., Rucci, M., & Poletti, M. (2022). Eye drift during fixation predicts visual acuity. *Proceedings of the National Academy of Sciences of the United States of America, 119*, 1–10.

Crane, H. D., & Steele, C. (1985). Generation V Dual Purkinje-Image eyetracker. *Applied Optics, 24*, 527–537.

De Lange Dzn, H. (1954). Relationship between critical flicker-frequency and a set of low-frequency characteristics of the eye. *Journal of the Optical Society of America, 44*, 380.

Derrington, A. M., & Lennie, P. (1984). Spatial and temporal contrast sensitivities of neurones in lateral geniculate nucleus of macaque. *Journal De Physiologie, 357*, 219–240.

Desbordes, G., & Rucci, M. (2007). A model of the dynamics of retinal activity during natural visual fixation. *Visual Neuroscience, 24*, 217–230.

Engbert, R., Mergenthaler, K., Sinn, P., & Pikovsky, A. (2011). An integrated model of fixational eye move- ments and microsaccades. *Proceedings of the National Academy of Sciences of the United States of America, 108*, 765–770.

Gur, M. (2024). Seeing on the fly: Physiological and behavioral evidence show that space-to-space representation and processing enable fast and efficient performance by the visual system. *Journal of Vision, 24*, 1–11, doi:10.1167/jov.24.11.11.

Hecht, S., & Shlaer, S. (1936). Intermittent stimulation by light: V. The relation between intensity and critical frequency for different parts of the spectrum. *Journal of General Physiology, 19*, 965–977.

Hong, G., Gan, X., Leonhardt, C., Zhang, Z., Seibert, J., Busch, J. M., . . . Bräse, S. (2011). A brief history of oleds—emitter development and industry milestones. *Advanced Materials, 33*, 2005630.

Intoy, J., Li, Y. H., Bowers, N. R., Victor, J. D., Poletti, M., & Rucci, M. (2024). Consequences of eye movements for spatial selectivity. *Current Biology, 34*, 3265–3272.

Intoy, J., & Rucci, M. (2020). Finely tuned eye movements enhance visual acuity. *Nature Communications, 11*, 1–11.

Kaplan, E., & Benardete, E. (2001). The dynamics of primate retinal ganglion cells. *Progress in Brain Research, 134*, 17–34.

Kobayashi, S., Miyama, T., Akiyama, H., Ikemura, A., & Kitamura, M. (2022). Development of liquid crystal displays and related improvements to their performances. *Proceedings of the Japan Academy, Series B, 98*, 493–516.

Kowler, E. (2011). Eye movements: The past 25 years. *Vision Research, 51*, 1457–1483.

Kuang, X., Poletti, M., Victor, J. D., & Rucci, M. (2012). Temporal encoding of spatial information during active visual fixation. *Current Biology, 20*, 510–514.

Li, Y. H., Cox, M., Victor, J., & Rucci, M. (2025). What one sees depends on how far the eye has moved. *BioRxiv*, https://www.biorxiv.org/content/10.1101/2025.09.17.676280v1.

Lin, Y., Intoy, J., Clark, A. M., Rucci, M., & Victor, J. D. (2023). Cognitive influences on fixational eye movements. *Current Biology, 33*, 1606–1612.

Marshall, W. H., & Talbot, S. A. (1942). Recent evidence for neural mechanisms in vision leading to a general theory of sensory acuity. In H. Kluver (Ed.), *Biological dymposia—visual mechanisms* (*Vol. 7*, pp. 117–164), Lancaster, PA: Cattel.

Mostofi, N., Boi, M., & Rucci, M. (2016). Are the visual transients from microsaccades helpful? Measuring the influences of small saccades on contrast sensitivity. *Vision Research, 118*, 60–69.

Poletti, M., & Rucci, M. (2016). A compact field guide to the study of microsaccades: Challenges and functions. *Vision Research, 118*, 83–97.

Purpura, K., Tranchina, D., Kaplan, E., & Shapley, R. M. (1990). Light adaptation in the primate retina: Analysis of changes in gain and dynamics of monkey retinal ganglion cells. *Visual Neuroscience, 4*, 75–93.

Ratnam, K., Domdei, N., Harmening, W. M., & Roorda, A. (2017). Benefits of retinal image motion at the limits of spatial vision. *Journal of Vision, 17*, 30, doi:10.1167/17.1.30.

Rucci, M., Ahissar, E., & Burr, D. (2018). Temporal coding of visual space. *Trends in Cognitive Sciences, 22*, 883–895.

Rucci, M., Iovin, R., Poletti, M., & Santini, F. (2007). Miniature eye movements enhance fine spatial detail. *Nature, 447*, 852–855.

Rucci, M., & Poletti, M. (2015). Control and function of fixational eye movements. *Annual Review of Vision Science, 1*, 499–518.

Rucci, M., & Victor, J. D. (2015). The unsteady eye: An information processing stage, not a bug. *Trends in Neurosciences, 38*, 195–206.

Santini, F., Redner, G., Iovin, R., & Rucci, M. (2007). EyeRIS: A general-purpose system for eye movement contingent display control. *Behavior Research Methods, 39*, 350–364.

Sperling, G. (1971). Flicker in computer-generated visual displays—selecting a cro phosphor and other problems. *Behavior Research Methods, Instruments, & Computers, 3*, 151–153.

Victor, J. D. (1987). The dynamics of the cat retinal X cell center. *Journal de Physiologie, 386*, 219–246.

Watson, A. (2014). A formula for human retinal ganglion cell receptive field density as a function of visual field location. *Journal of Vision, 14*, 1–17, doi:10.1167/14.7.15.

Wu, E. G., Brackbill, N., Rhoades, C., Kling, A., Gogliettino, A. R., Shah, N. P., . . . Chichilnisky, E. J. (2024). Fixational eye movements enhance the precision of visual information transmitted by the primate retina. *Nature Communications, 15*, 1–15.

Wu, R.-J., Clark, A. M., Cox, M. A., Intoy, J., Jolly, P. C., Zhao, Z., . . . Rucci, M. (2023). High-resolution eye-tracking via digital imaging of Purkinje reflections. *Journal of Vision, 23*, 1–17, doi:10.1167/jov.23.5.4.

Yang, B., Intoy, J., & Rucci, M. (2024). Eye blinks as a visual processing stage. *Proceedings of the National Academy of Sciences of the United States of America, 121*, e2310291121.

Yang, B., Victor, J., & Rucci, M. (2025). Residual foveal motion facilitates processing of visually tracked objects. *BioRxiv*, https://www.biorxiv.org/content/10.1101/2025.09.18.677233v1.